Chaos and order of laser-cooled ions in a Paul trap

R. Blümel, C. Kappler, W. Quint, and H. Walther
Max-Planck-Institut für Quantenoptik and Sektion Physik, Universität München, D-8046 Garching, Federal Republic of Germany
(Received 18 January 1989)

We present recent experimental and theoretical results on the behavior of two-, three-, and four-ion crystals close to the Mathieu instability. In particular, we show that the crystals are stable until the Mathieu instability is reached, i.e., for the parameter space investigated, there is no "melting" of the crystals. Laser and rf heating are studied in detail. A simple model of chaotic rf heating as well as a classification of the ion dynamics into four characteristic regimes are presented.

I. INTRODUCTION

For centuries the study of nonlinear systems has been neglected because it was thought that every given nonlinear system needs its own individual method of solution. In such a case not much can be learned for the set of all nonlinear systems by considering only one. Moreover, the solutions of nonlinear systems tend to be very complicated, in some cases even leading to chaos. A substantial breakthrough occurred when Feigenbaum showed some ten years ago[1] that there is *universality* in chaos and that much can be learned about the class of nonlinear systems by studying only a few representative examples. Since then, researchers have concentrated on the study of kicked systems[2–8] and the continuously driven hydrogen atom.[9–13] Although quite different, these physical systems can be treated in a unified way using the new language of "chaos" and "localization" theory.

In this paper we discuss yet another physical system which shows all the standard features of chaos: laser-cooled ions confined in the dynamical potential of a Paul trap. It appears that recently observed dynamical effects exhibited by trapped laser-cooled ions are purely classical in origin and can be attributed to the occurrence of chaos in the ion dynamics.[14–17] With laser-cooled ions it is possible to reach the quantum limit[18] and thus to challenge the monopoly of hydrogen and alkali-metal Rydberg atoms perturbed by strong electromagnetic fields as the experimental paradigms of quantum chaos research.[9–13,19,20]

In connection with crystallized beams in storage rings, the investigation of the dynamics of trapped ions has gained additional relevance in recent years since a Paul trap can model confining forces and focusing sections in ion storage rings. The feasibility of crystallization in existing and planned heavy-ion storage rings is currently much debated,[21–24] and the experience accumulated by studying ion traps might be helpful for the production and diagnostics of Coulomb crystals in ion storage rings.

The paper is organized in the following way. After quickly reviewing the case of a single ion in a Paul trap and deriving the equations of motion for an arbitrary number of ions in the trap (Sec. II), we present a detailed study of the problem of two ions interacting via the repulsive Coulomb force and confined in the secular potential of the trap (Sec. III). The two-ion dynamics is treated in analogy to the Hénon-Heiles problem,[25] and we find that for almost all deformations of the secular potential chaos occurs as soon as the energy of the ions surpasses a critical value. For special nontrivial values of the deformation, the equations of motion of the two ions are integrable due to the existence of accidental constants of the motion, which can be calculated analytically. The recently suggested mechanism of chaotic ion melting[14] is the subject of Sec. IV. Searching for this mechanism, we investigate in detail the behavior of two-, three-, and four-ion crystals close to the Mathieu instability (MI). We present experimental and theoretical material which supports our early numerical result that ion crystals are stable until the MI is reached,[15] i.e., in the parameter regime investigated, there is no chaotic ion melting. In Sec. V we investigate a mechanism of ion heating[26] and cooling which relies on the micromotion of the ions. Section VI, finally, presents a simple model of chaotic rf heating which explains the sharpness and reproducibility of the observed cloud→crystal phase transitions.[15–17,27] It is also demonstrated that the ion dynamics in a Paul trap can be classified into four dynamical regimes.[16,17] This classification seems to be rather universal and shows up in the dynamics of periodically perturbed polar molecules,[4] the hydrogen atom in strong magnetic fields,[28] and the periodically perturbed hydrogen atom.[11,29]

II. IONS IN A PAUL TRAP: BASIC EQUATIONS

The equations of motion of a single ion in the dynamical quadrupole potential

$$\phi^{(\mathrm{trap})}(x,y,z)=\frac{U_0+V_0\cos(\Omega t)}{r_0^2+2z_0^2}(x^2+y^2-2z^2) \qquad (1)$$

of a Paul trap are given by[30–33]

$$m\frac{d^2}{dt^2}\begin{bmatrix}x\\y\\z\end{bmatrix}=2e\frac{U_0+V_0\cos(\Omega t)}{r_0^2+2z_0^2}\begin{bmatrix}x\\y\\-2z\end{bmatrix}=0\ . \qquad (2)$$

In the above equations U_0 and V_0 are the dc and ac parts of the trap potential, r_0 is the radius of the ring electrode,

and z_0 is half the distance between the end caps of the trap. The mass of the ion is denoted by m, and e is the elementary charge. Introducing dimensionless constants

$$a=\frac{8eU_0}{m\Omega^2(r_0^2+2z_0^2)},\quad q=\frac{4eV_0}{m\Omega^2(r_0^2+2z_0^2)} \tag{3}$$

and dimensionless time

$$\tau=\Omega t/2\ , \tag{4}$$

the equations of motion (2) are transformed to the standard form of three uncoupled Mathieu-type equations corresponding to the motion in the three principal axes of the trap:

$$\frac{d^2}{d\tau^2}\begin{bmatrix}x\\y\\z\end{bmatrix}+[a+2q\cos(2\tau)]\begin{bmatrix}x\\y\\-2z\end{bmatrix}=0\ . \tag{5}$$

This set of equations has been studied in detail in the literature, and it is known that depending on a and q, Eq. (5) possesses bounded (stable) and unbounded (unstable) solutions. Figure 1 shows a section of the a-q stability plane. In the range of a and q values shown here, stable motion is encountered only in the regions A and B, whereas all the other displayed a-q combinations will lead to unbounded motion. In this connection, we can mention an interesting possibility for further research: In all the ion-trap experiments reported so far, the traps were always operated in stability region A. Operating the trap in region B requires more voltage applied to the trap, but, on the other hand, perturbative approaches are no longer valid in region B, offering interesting consequences for the ion dynamics. Preliminary numerical investigations of region B indicate that most probably ion crystals are not stable in this region unless one invests an excessive amount of cooling power.

It is important to note that different research groups have worked with different ion species (e.g., He,[33] Ba,[14] Mg,[15–17,27] Hg,[34] etc.), but due to classical scaling, the equations of motion (5) depend only on the dimensionless parameters a and q and thus the results obtained by different groups can nevertheless be compared directly. This is no longer true in the quantum limit, where $\hbar$ sets an absolute scale.

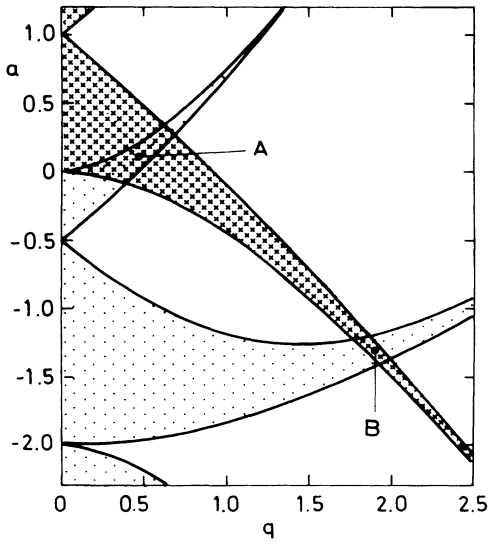

FIG. 1. Stability diagram of the Paul trap.

Consider the x component of (5):

$$\ddot{x}+[a+2q\cos(2\tau)]x=0\ . \tag{6}$$

This is a linear differential equation with a periodic coefficient, and Floquet's theorem[35] tells us that the solutions are of the form

$$x(\tau)=Q(\tau)\Phi(\tau)\ , \tag{7}$$

where $Q(\tau)=e^{i\mu\tau}$ represents the slow motion, or secular motion, and $\Phi(\tau)$ is a π-periodic function representing the so-called micromotion. In the unstable regimes of the stability diagram displayed in Fig. 1, μ is a complex number with a negative imaginary part resulting in exponentially unstable motion. For real μ, the orbit $x(\tau)$ is quasiperiodic (stable) and, to lowest approximation in small a and q, is given by

$$x=x_0\left[1+\frac{q}{2}\cos(2\tau)\right]e^{i\mu_x\tau}\ , \tag{8}$$

where the amplitude x_0 is determined by the initial conditions and

$$\mu_x=(a+\tfrac{1}{2}q^2)^{1/2}\ . \tag{9}$$

The angular frequency of the secular motion in the original units is then given by

$$\omega_x=\mu_x\frac{\Omega}{2}\ , \tag{10}$$

and since for the z equation $q\rightarrow -2q$, $a\rightarrow -2a$, we have

$$\mu_z=[2(q^2-a)]^{1/2},\quad \omega_z=\mu_z\frac{\Omega}{2}\ . \tag{11}$$

Let us emphasize again that (8)–(11) are only valid for $a,q\ll 1$, and they are, e.g., completely invalid in region B of Fig. 1.

The secular motion allows a rewriting of the equation of motion (6):

$$\ddot{x}+\mu_x^2x+f(\tau)x=0\ , \tag{12}$$

where f is the residual interaction

$$f(\tau)=2q\cos(2\tau)-\tfrac{1}{2}q^2\ , \tag{13}$$

which is responsible for the micromotion of the ions. Equation (12) shows quite clearly the decomposition of the motion into a slowly oscillating part with frequency μ_x and a fast parametric drive with

$$\langle f(\tau)\rangle=\frac{1}{\pi}\int_0^{\pi}f(\tau)x(\tau)d\tau=0\ . \tag{14}$$

The above equation shows that the micromotion part is a term in the equation of motion which "averages out."

Let us now switch on the Coulomb force and calculate

the equilibrium separation d_0 of two ions confined by the secular oscillator. For $a<q^2/2$, the ions will lie in the $z=0$ plane. Equating the restoring force of the pseudo-oscillator

$$F_{\rm osc}=m\omega_x^2\frac{d}{2} \tag{15}$$

and the Coulomb force acting between the two ions,

$$F_{\rm Coul}=\frac{e^2}{4\pi\epsilon_0}\frac{1}{d^2}\ , \tag{16}$$

we arrive at

$$d_0=\left[\frac{2e^2}{m\pi\epsilon_0\Omega^2(a+\frac{1}{2}q^2)}\right]^{1/3}\approx\frac{40\ \mu{\rm m}}{[MF^2(2a+q^2)]^{1/3}}\ , \tag{17}$$

where M denotes the mass m of either of the two ions in atomic mass units and F is the trap frequency in MHz. The micromotion will explore the nonlinearities of the Coulomb potential resulting in an equilibrium distance d_0 which is somewhat larger than this simple estimate. Formula (17) can be checked experimentally as a function of a and q in the form $d_0^3(2a+q^2)=$const. For $a>q^2/2$, the ions will lie on the z axis and a similar derivation yields in this case

$$d_0=\left[\frac{e^2}{m\pi\epsilon_0\Omega^2(q^2-a)}\right]^{1/3}\approx\frac{25\ \mu{\rm m}}{[MF^2(q^2-a)]^{1/3}}\ . \tag{18}$$

We can also calculate the breathing-mode frequency of two ions, i.e., the frequency of small oscillations of d around d_0:

$$\begin{aligned}F_{\rm osc}(d_0+\Delta d)-F_{\rm Coulomb}(d_0+\Delta d)&=\tfrac{3}{2}m\omega_x^2\Delta d\\&=3m\omega_x^2\Delta x\end{aligned} \tag{19}$$

from which we read off the breathing-mode angular frequency

$$\omega_b=\sqrt{3}\omega_x\ . \tag{20}$$

In order to check these expressions we have applied an additional ac voltage of 15 mV amplitude to the trap whose frequency was varied between 100 and 400 kHz. This way the secular and breathing-mode frequencies can be resonantly excited, which destroys the two-ion equilibrium configuration. Experimentally the destruction happens for frequencies $f=170$, 280, and 350 kHz.[15] For the trap we have $r_0=2.5$ mm, $z_0=1.77$ mm, and $f=11.25$ MHz. For $U_0=0$ and $V_0=165$ V, we obtain

$$f_x=\frac{\omega_x}{2\pi}=170\ {\rm kHz},\quad f_z=\frac{\omega_z}{2\pi}=340\ {\rm kHz}\ ,$$

$$f_b=\frac{\omega_b}{2\pi}=\sqrt{3}f_x=280\ {\rm kHz}\ ,$$

which checks well with the experimental results.

As a next step, we derive the three-dimensional set of equations of motion of an arbitrary number of ions in a Paul trap. Measuring distances in units of the equilibrium distance d_0, we obtain

$$\begin{aligned}\frac{d^2}{d\tau^2}\begin{bmatrix}x_i\\y_i\\z_i\end{bmatrix}+[a+2q\cos(2\tau)]\begin{bmatrix}x_i\\y_i\\-2z_i\end{bmatrix}\\=\tfrac{1}{2}(a+\tfrac{1}{2}q^2)\sum_{\substack{i,j\\j\neq i}}\frac{\mathbf{x}_i-\mathbf{x}_j}{|\mathbf{x}_i-\mathbf{x}_j|^3}\ .\end{aligned} \tag{21}$$

In analogy to (12) we introduce the secular oscillator on the left-hand side of (21) and neglect the residual interaction:

$$\frac{d^2}{d\tau^2}\begin{bmatrix}x_i\\y_i\\z_i\end{bmatrix}+\begin{bmatrix}\mu_x^2x_i\\\mu_x^2y_i\\\mu_z^2z_i\end{bmatrix}=\tfrac{1}{2}\mu_x^2\sum_{\substack{i,j\\j\neq i}}\frac{\mathbf{x}_i-\mathbf{x}_j}{|\mathbf{x}_i-\mathbf{x}_j|^3}\ . \tag{22}$$

Specializing now to the case of two ions and introducing relative and center-of-mass (c.m.) coordinates

$$\mathbf{r}=\begin{bmatrix}x\\y\\z\end{bmatrix}=\mathbf{x}_1-\mathbf{x}_2,\mathbf{R}=\begin{bmatrix}X\\Y\\Z\end{bmatrix}=\tfrac{1}{2}(\mathbf{x}_1+\mathbf{x}_2)\ , \tag{23}$$

the equations of motion (21) separate into

$$\frac{d^2}{d\tau^2}\begin{bmatrix}x\\y\\z\end{bmatrix}+[a+2q\cos(2\tau)]\begin{bmatrix}x\\y\\-2z\end{bmatrix}=\mu_x^2\frac{\mathbf{r}}{|\mathbf{r}|^3}\ , \tag{24a}$$

$$\frac{d^2}{d\tau^2}\begin{bmatrix}X\\Y\\Z\end{bmatrix}+[a+2q\cos(2\tau)]\begin{bmatrix}X\\Y\\-2Z\end{bmatrix}=0\ . \tag{24b}$$

While the equations of motion (24b) represent three uncoupled Mathieu-type equations for the c.m. motion, Eqs. (24a) for the relative motion are nonlinear coupled equations, which can lead to chaos[14–17] and therefore cannot be solved analytically. Introducing the secular oscillator into (24a) and (24b), we obtain

$$\frac{d^2}{d\tau^2}\begin{bmatrix}r_x\\r_y\\r_z\end{bmatrix}+\begin{bmatrix}\mu_x^2r_x\\\mu_x^2r_y\\\mu_z^2r_z\end{bmatrix}=\mu_x^2\frac{\mathbf{r}}{|\mathbf{r}|^3}\ , \tag{25a}$$

$$\frac{d^2}{d\tau^2}\begin{bmatrix}R_x\\R_y\\R_z\end{bmatrix}+\begin{bmatrix}\mu_x^2R_x\\\mu_x^2R_y\\\mu_z^2R_z\end{bmatrix}=0\ . \tag{25b}$$

This time, the c.m. motion splits into three decoupled oscillator equations which are trivially solvable. We introduce polar coordinates in the x-y plane

$$r_x=\rho\cos\phi,\quad r_y=\rho\sin\phi,\quad r_z=\zeta\ . \tag{26}$$

Because of the axial symmetry of the trap,

$$L_z=\rho^2\dot{\phi} \tag{27}$$

is a constant of the motion and the remaining equations to be solved are

$$\ddot{\rho}-\frac{L_z^2}{\rho^3}+\mu_x^2\rho=\mu_x^2\frac{\rho}{(\rho^2+\zeta^2)^{3/2}}\ , \tag{28a}$$

$$\ddot{\zeta}+\mu_z^2\zeta=\mu_x^2\frac{\zeta}{(\rho^2+\zeta^2)^{3/2}}\ . \tag{28b}$$

Scaling the time to match the secular oscillations, the final set of equations of motion is given by

$$\ddot{\rho}-\frac{\nu^2}{\rho^3}+\rho=\frac{\rho}{(\rho^2+\zeta^2)^{3/2}}\ , \tag{29a}$$

$$\ddot{\zeta}+\lambda^2\zeta=\frac{\zeta}{(\rho^2+\zeta^2)^{3/2}}\ , \tag{29b}$$

which can be derived from the Hamiltonian

$$H=\frac{p_\rho^2}{2}+\frac{p_\zeta^2}{2}+V(\rho,\zeta)\ ,$$
$$V(\rho,\zeta)=\tfrac{1}{2}\rho^2+\tfrac{1}{2}\lambda^2\zeta^2+\frac{\nu^2}{2\rho^2}+\frac{1}{(\rho^2+\zeta^2)^{1/2}}\ , \tag{30}$$

where $p_\rho=\dot{\rho}$, $p_\zeta=\dot{\zeta}$, and $\nu=L_z/\mu_x$ and $\lambda=\mu_z/\mu_x$ are the dimensionless control parameters. The parameter λ describes the deformation of the secular oscillator and is real and positive in the stability regions of the a,q stability chart (see Fig. 1). At the MI or, generally, in the unstable regions of the trap, λ is purely imaginary, so that λ^2 is negative, which results in an inverted harmonic oscillator on the left-hand side of (29b) and leads to an unstable situation. For $\lambda=1$ the secular oscillator is spherical, for $\lambda<1$ it is steeper in the ρ direction, and for $\lambda>1$ it is steeper in the ζ direction. Equipotential lines of the potential $V(\rho,\zeta)$ are shown in Fig. 2.

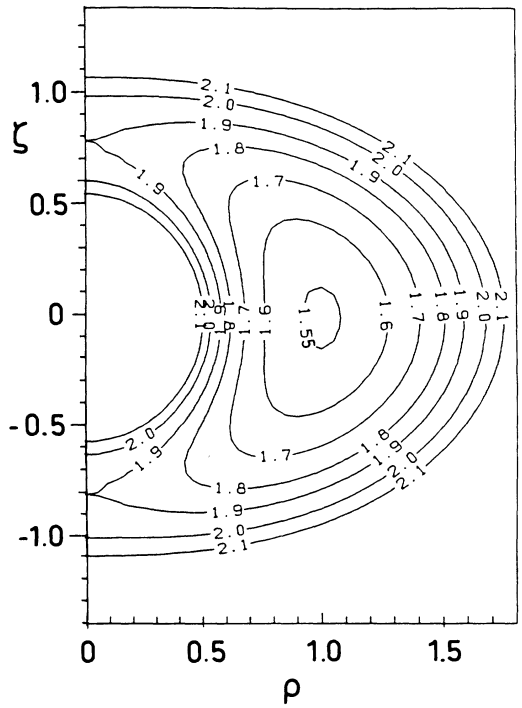

FIG. 2. Equipotential lines of the pseudopotential $V(\rho,\zeta)$ [defined in (30)] for $\lambda=\sqrt{2}$ and $\nu=0$. The axes are in units of the equilibrium distance d_0.

For $\lambda>1$ the potential V exhibits a minimum (located on the ρ axis) and two saddle points (located on the ζ axis). For $E=E_{\min}=\frac{3}{2}$, we have $\rho\equiv1$, which corresponds to the crystalline solution, where the ions are separated by one unit of equilibrium distance d_0.

III. CHAOS AND ORDER OF TWO IONS IN THE SECULAR OSCILLATOR POTENTIAL

The solutions of (29) are Newtonian trajectories in four-dimensional phase space. But since the coupled equations (29) do not explicitly depend on time, the Hamiltonian (30) H is a constant of the motion. For given energy $E=H$, the trajectories are therefore confined to a three-dimensional hypersurface. Visualization of the trajectories is greatly simplified if—in analogy to the Hénon-Heiles problem[25]—we introduce a Poincaré surface of section.[36] This means that we plot a point in the x-y plane whenever the trajectory fulfills the condition

$$p_\rho=0,\quad p_\zeta>0\ . \tag{31}$$

This is done for different initial conditions. Regular motion corresponds to a regular pattern of points, whereas chaotic motion corresponds to a disordered set of points.

A special situation occurs for $\lambda=1$. In this case the secular oscillator is spherical, the total angular momentum of the ions $\mathbf{L}$ is a constant, and the equations of motion in this case are completely integrable. For $\lambda\neq1$ the situation is not so trivial. Figure 3 shows Poincaré surfaces of section surrounded by the equipotential line for $\lambda=\sqrt{2}$, $\nu=0$, and three different energies. For $1.5<E\leq1.60$ we see that essentially all phase-space trajectories are regular [see Fig. 3(a)], but one can already find some small "islands" which arise from only one initial condition and surrounding fixed points, i.e., resonances. According to the Kol'mogorov-Arnold-Moser (KAM) theorem these resonances are the first structures to break up.[36] This can be seen for $E=1.65$ [Fig. 3(b)], where a small fraction of phase space is already chaotic and at $E=1.8$ [Fig. 3(c)] chaos prevails. For high energies the motion becomes regular again, because the nonlinearities of the potential are not felt any more (Mathieu regime).

This behavior is found for all ν and all λ, except for $\lambda=2$ and $\lambda=\frac{1}{2}$. Here all trajectories at any energy are regular. This points to the existence of an additional constant of the motion (COM) besides the energy, which confines the trajectories to a two-dimensional hypersurface, whose section with the two-dimensional Poincaré surface of section results in one-dimensional curves.

In order to find the COM's, we exploit the similarity between the present problem and the hydrogen atom. We first concentrate on the case $\nu=0$ and try to construct the COM's from the various components of

$$\mathbf{I}=\mathbf{R}+\mathbf{C}(\rho,\zeta)\ , \tag{32}$$

where

$$\mathbf{R}=\mathbf{v}\times\mathbf{L}+\frac{\mathbf{r}}{|\mathbf{r}|} \tag{33}$$

is the Runge-Lenz vector which is a COM for potentials $V \sim 1/r$, and **C** is assumed to depend only on the position coordinates. The velocity coordinates are assumed to be taken care of by the Runge-Lenz vector, which is the essence of the ansatz. The total time derivative of (32) vanishes if

$$\dot{C}_\rho = (1-2\lambda^2)\rho\zeta\dot{\zeta} + \lambda^2\zeta^2\dot{\rho} \ , \tag{34a}$$

$$\dot{C}_\zeta = (\lambda^2-2)\zeta\rho\dot{\rho} + \rho^2\dot{\zeta} \ . \tag{34b}$$

The function C_ρ is a total differential if and only if $\lambda=\frac{1}{2}$, and C_ζ if and only if $\lambda=2$. Therefore, in the two-dimensional case and for $\lambda=\frac{1}{2}$, the ζ component of **I** is a COM and for $\lambda=2$ it is the ρ component:

$$I_\rho^{(\nu=0)} = \rho\dot{\zeta}^2 - \dot{\rho}\zeta\dot{\zeta} + \frac{\rho}{(\rho^2+\zeta^2)^{1/2}} - \tfrac{1}{4}\zeta^2\rho \ , \tag{35a}$$

$$I_\zeta^{(\nu=0)} = \zeta\dot{\rho}^2 - \dot{\zeta}\rho\dot{\rho} + \frac{\zeta}{(\rho^2+\zeta^2)^{1/2}} - \rho^2\zeta \ . \tag{35b}$$

A generalization to three dimensions (i.e., $\nu\neq 0$), which yields another term in the equations of motion, results for $\lambda=2$ just in an additional term (proportional to ν^2) in I_ζ, and the COM, in this case F, is given by

$$F(\rho,\dot{\rho},\zeta,\dot{\zeta};\nu) = I_\zeta^{(\nu=0)} + \frac{\nu^2}{\rho^2} \ . \tag{36}$$

The COM for $\lambda=\frac{1}{2}$, G, is obtained from the length of the vector **I** in the x-y plane. We obtain

$$G(\rho,\dot{\rho},\zeta,\dot{\zeta};\nu) = I_\rho^{(\nu=0)^2} + I_\phi^{(\nu=0)^2} + \nu^2(\rho^2+\zeta^2) \ , \tag{37}$$

where $I_\rho^{(\nu=0)}$ was defined in Eq. (35a) and $I_\phi^{(\nu=0)}$ is given by

$$I_\phi^{(\nu=0)} = R_\phi = -\frac{\nu}{\rho}(\rho\dot{\rho} + \zeta\dot{\zeta}) \ . \tag{38}$$

It is possible that the existence of the constants of the motion for $\lambda=2$ and $\lambda=\frac{1}{2}$ results in additional stability of the two-ion dynamics even if the micromotion is not neglected. Experiments addressing this point are now in progress.[37]

Coming back to the equations of motion (29), we notice that their structure does not change as long as a and q are chosen from the stable regions of the stability diagram. This means that the chaos scenario depicted in Fig. 3 is qualitatively the same for all of these a and q values and changes drastically only if (a,q) is chosen from an unstable region of the stability chart. Therefore, on the basis of the calculations presented in this section, we cannot identify any "special" values of a and q at which the dynamics of two-ion crystals would change suddenly, and which could perhaps be identified as order→chaos transitions in the control parameter q, as suggested in Ref. 14. Quite the contrary; due to the structural invariance of Eqs. (29), we are led to the conclusion that in the absence of micromotion, two-ion crystals are stable until the MI is reached. That this holds even in the presence of the micromotion, i.e., for the realistic system without any approximations, is demonstrated in Sec. IV.

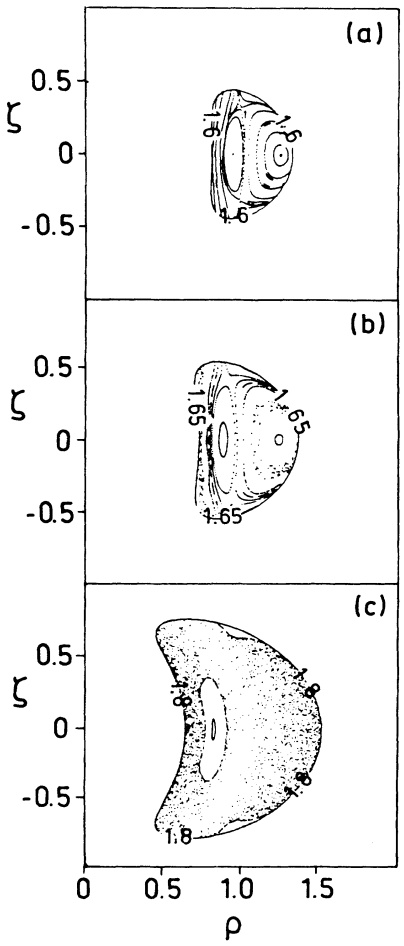

FIG. 3. Poincaré surfaces of section showing the transition to global stochasticity for the dimensionless equations of motion (29). (a) $E=1.6$, (b) $E=1.65$, and (c) $E=1.8$.

IV. THE CRYSTAL→CLOUD TRANSITION

In order to prove that there is no order→chaos transition, but instead that the crystal is surrounded by quasiperiodic solutions of the coupled equations of motion (21), we have investigated the sensitivity of ion crystals, consisting of up to five ions, to radial and axial displacements by adding spontaneous-emission noise.[15–17] No melting of the crystals was observed. Since in actual experiments the presence of contact potentials cannot be avoided, we have also investigated the stability of two-ion crystals subjected to spontaneous-emission noise and contact potentials which produced electric fields of the order of 200 mV/cm in the x-y plane and 100 mV/cm in the z direction. Even in the presence of these additional forces, our three-dimensional (3D) simulations did not show any sign of crystal melting, and as a function of the ac voltage applied to the trap, the two-ion crystals turned out to be stable until the MI was reached.

A quantitative measure of the sensitivity of a two-ion crystal to displacements in the z direction is obtained by starting out in the crystal solution and displacing one of

the two ions in the crystalline phase a distance δz out of equilibrium. This new situation serves as an initial condition for the solution of the equations of motion (21). (No laser cooling is present for this type of calculation.) Depending on the magnitude of δz, the new configuration leads to two possible behaviors: (i) quasiperiodic motion, i.e., a motion whose Fourier spectrum exhibits a sequence of sharp lines (the nonheating phase), (ii) heating, which finally results in a two-ion cloud. The line in Fig. 4 separates region (i) from region (ii). This line cuts the q axis only at $q=q_{\mathrm{MI}}$ and provides strong evidence that there is no order→chaos transition following any of the standard scenarios, since otherwise the line should have cut the q axis at $q_c < q_{\mathrm{MI}}$.

A more complete investigation of this point should concentrate on the structure of the phase space surrounding the phase-space domain which corresponds to a two-ion crystal. Let us assume that no angular momentum is present and that the phase of the rf driving field is fixed as in (24), i.e., the argument of the cosine is 0 for $\tau=0$. If we check the position of a two-ion crystal under these conditions at discrete times $\tau=0,\pi,2\pi,\ldots$, we will find $x\approx 1$, $z=0$ and $\dot{x}\approx 0$, $\dot{z}\approx 0$. We now explore the stability of phase-space points Q surrounding the point $C=(x,z,\dot{x},\dot{z})\approx(1,0,0,0)$, which corresponds to the two-ion crystal. The vicinity of C is, of course, four dimensional, and we restrict our investigation to a two-dimensional cut which is defined by $\dot{x}(0)=0$ and $\dot{z}(0)=0$. For time $\tau=0$, we choose a point Q from the phase-space region $0\le x\le 2.2$, $0\le z\le 0.2$, $\dot{x}=\dot{z}=0$, which serves as an initial condition for the solution of the equations of motion (24a), which are integrated forward in time for 100 rf cycles. During the integration it is checked whether the two ions gain energy, or whether their energy stays constant. The two cases turned out to be easily distinguishable, since in the former case, the time-averaged kinetic energy $E_{\mathrm{kin}}=\frac{1}{2}(\dot{\rho}^2+\dot{\zeta}^2)$ always turned out to be of the order of 1, whereas in the latter case it was bounded and $E_{\mathrm{kin}}\sim 10^{-3}$. We therefore chose a dividing line of $E_{\mathrm{kin}}=5\times 10^{-3}$ to distinguish between phase-space points which correspond to the nonheating and heating phases, respectively. Figure 5(a) shows the result of this numerical experiment for $a=0$ and $q=0.452$, which is very close to the MI and much larger than $q=0.425$, which was claimed to be the point which corresponds to the onset of chaotic motion in Ref. 14. The black dots corre-

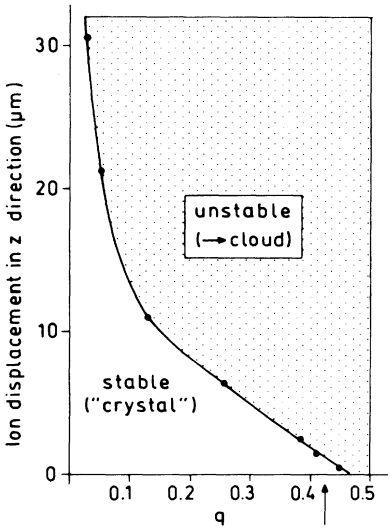

FIG. 4. Sensitivity of a two-ion crystal to displacements in z direction as a function of q. The crystal lies initially in the x-y plane. Then, one of the ions is displaced in the z direction which defines the initial condition for (29). Depending on its magnitude this initial displacement can either lead to crystals or to clouds. The solid curve marks the boundary between these two regions. The arrow points to the q value at which according to Ref. 14 the two-ion crystal should melt.

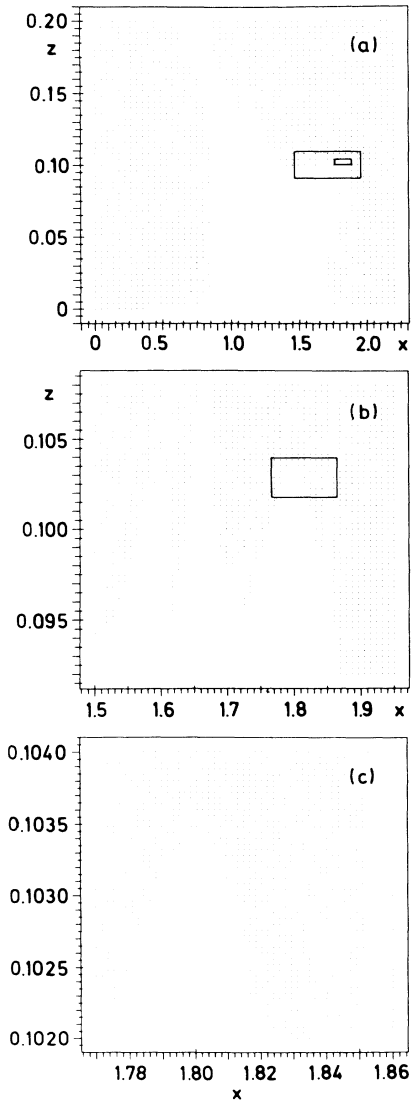

FIG. 5. Heating (black dots) and nonheating (white regions) areas of a section of two-ion phase space. (b) and (c) are successive magnifications of the areas in (a) marked by the large and the small rectangle, respectively. Structure is apparent on all scales indicating that the boundary surface separating heating and nonheating phase-space areas shows fractal character.

spond to initial conditions which show heating and which, after 100 rf cycles, have already developed into a cloud state. The white region does not show any heating. Figure 5(a) shows that the stability region around the two-ion crystal is in fact two dimensional (within the chosen cut) and no order→chaos transition can take place. It is also interesting that the boundary between the stable and unstable region seems to have a very complicated structure. In order to investigate this further, Fig. 5(b) shows a magnified picture of the region in phase space which is marked by the large rectangle in Fig. 5(a). A further magnification [the small rectangle in Fig. 5(a)] is shown in Fig. 5(c). It is interesting that there seems to be structure on all scales and the phase-space boundary between crystals and clouds shows fractal character.[25,38,39] In any case, Figs. 4 and 5(a) provide clear evidence that the interpretation of the crystal→cloud transition as an order→chaos transition in the control parameter q, which was put forward by the authors of Ref. 14, is at least questionable.

This is also demonstrated by our experiments.[37] We investigated carefully the behavior of a single ion, and two-, three-, and four-ion crystals close to the MI, which for $a=0$ occurs at $q=0.454$. To this aim, we load single ions or crystals at $q=0.15$ and increase q adiabatically in about 5 sec to $q=0.5(dq/d\tau=2\times10^{-9})$. As a function of q, we record the fluorescence intensity at a detuning of $\Delta=-200$ MHz and laser power $P=100\ \mu$W. Figure 6(a) shows that the fluorescence intensity in the single-ion case drops to zero exactly at the expected $q=q_{\mathrm{MI}}$. For comparison, Fig. 6(b) shows that even in the two-ion case, the fluorescence, and therefore the crystal, survives until $q=q_{\mathrm{MI}}$ is reached. This shows clearly that a two-ion crystal, even in the presence of spontaneous-emission noise, did not melt until the MI was reached. Of course, due to uncontrollable sources of technical noise, the "melting" points of the ion crystals scatter considerably over relatively large ranges of q. This we noticed already in earlier work on this subject, e.g., in Ref. 15, Fig. 3, which shows a five-ion crystal "melting" at $q<q_{\mathrm{MI}}$.

Figure 7 displays all our experimentally obtained crystal→cloud transition points in the form of a histogram plot which shows the probability of occurrence of a transition as a function of q (bin size $\Delta q=0.005$) for several values of a and particle number n. For zero dc voltage and $n=2$, a large body of transition points occurs at q values which are substantially higher than the published value[14] of $q=0.425\pm0.005$ which was claimed to be the *reproducible* value of the onset of chaotic motion. Even for the case of three to five ions, the calculations predict that there is no chaotic ion melting and that ion crystals are stable even if laser cooling and spontaneous-emission noise are switched on.[15–17] Three-ion crystals are apparently more sensitive to perturbations since the

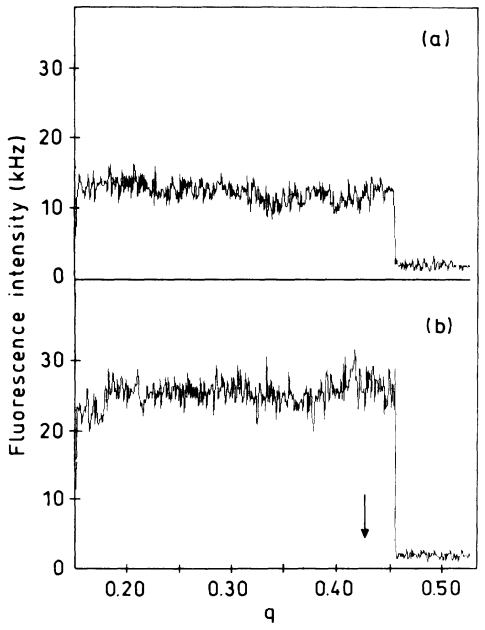

FIG. 6. A single scan of the fluorescence intensity (given in counts per second) of (a) a single-ion and (b) a two-ion crystal as a function of q for $a=0$. The fluorescence drops sharply at $q=q_{\mathrm{MI}}$ where both the single ion (a) and the crystal (b) fall out of the trap. The scan time for q was ≈5 sec. For the two-ion case, the crystalline structure is preserved up to $q=q_{\mathrm{MI}}$. The arrow marks the positions where, according to Ref. 14, the crystal→cloud transition should have occurred.

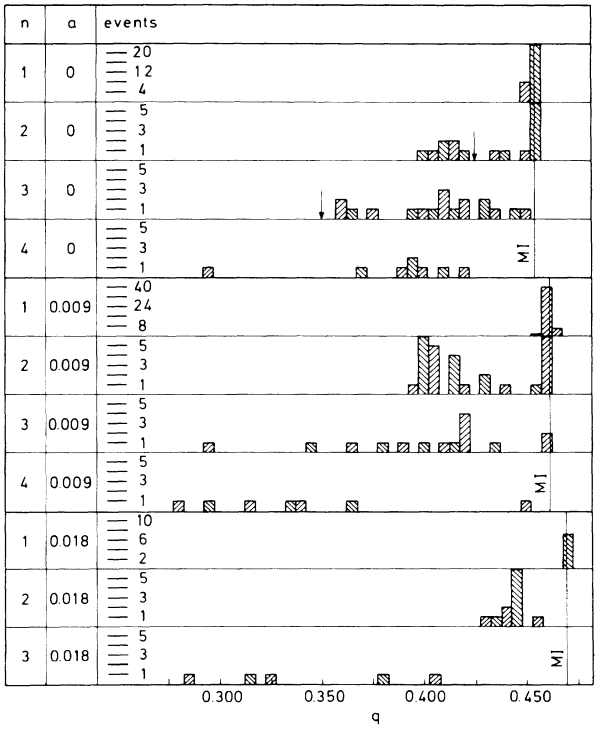

FIG. 7. Probability distribution of experimentally observed transition points for the crystal→cloud transition as a function of q and for several values of a and the ion number n. The plot was produced from a statistical basis of 200 investigated crystals. The arrows for $a=0$ and $n=2,3$ mark the q values where according to Ref. 14 the two- and three-ion crystals should have melted.

bulk of the three-ion transition points shown in Fig. 7 is lower than in the two-ion case. This behavior was also noted in Ref. 14, although our three-ion transition points occur at considerably larger q reaching up to $q=0.45$, very close to the MI. The results for four ions, also shown in this figure, reflect an even larger sensitivity and underline the general trend. We conclude that for zero dc voltage and without external technical noise, ion crystals are stable until the MI is reached, even in the presence of laser cooling which causes system-inherent perturbations, namely, spontaneous-emission noise.

The difference between the above results and those presented in Refs. 14 and 26 might be due to the following reasons. (i) The pressure of the background gas was reported in Ref. 14 to be 1.3×10^{-9} mbar, whereas in our experiments it is more than a factor of 6 better and amounts to 2×10^{-10} mbar. The lower pressure in our trap guarantees a lower collision rate of rest gas molecules with the stored crystals and hence a higher stability. (ii) Due to the slower q-scan time[26] in the experiments of Ref. 14, the ion crystals are exposed for a longer time to any perturbations which might melt the crystals. This, obviously, results in a shift of the statistics of "melting points" toward lower q values. (iii) In the calculations of Ref. 14, the authors implemented spatial displacement noise to describe the influence of spontaneous emission, whereas a more appropriate model would have been to use random noise in the momentum of the ions. Moreover, the initial conditions in the simulations reported in Ref. 14 were slightly displaced and not fully converged.[26]

Of course there is still a possibility of obtaining genuine order→chaos transitions for nonzero dc voltage. We have performed similar ion-melting experiments for 16- and 32-V dc voltage applied to the ring electrode of the trap. Even in this case, Fig. 7 shows that the experimentally obtained transition points are consistent with the claim[16,17] that ion crystals can be stable up to $q=q_{\mathrm{MI}}$.

The results displayed in Fig. 7 have been obtained using a specific value of the laser detuning and laser power $P\approx100$ μW. Since laser cooling is a highly nonlinear process, the question arises, whether for different values of the detuning and the laser power, or larger number of ions, ion crystals can be heated up, which would lead to the melting of the crystals. Remarks addressing this point have been put forward in Ref. 14 and on various other occasions.[26]

V. LASER COOLING AND LASER HEATING

Except for Ref. 26, the theory of laser cooling of ions stored in a Paul trap was treated only for ions confined in the secular pseudo-oscillator potential neglecting the micromotion. Since here we are interested in the behavior of stored ions close to the MI; the name "micromotion" is somewhat misleading, since in the two-ion case, the amplitude of the micromotion oscillations amounts to about 20% of the equilibrium separation of the ions. This micromotion can be seen in the modulation of the fluorescence intensity as reported earlier.[40] Here we discuss similar measurements with a two-ion crystal ($a=0$, $q=0.065$, $P=100$ μW, $\Delta=-150$ MHz). In contrast to Ref. 40, in the present work the time-to-amplitude converter (TAC) was triggered by the rf generator directly instead of using photon signals. The TAC was then stopped by the arrival of a fluorescence photon in the detector. The height of the output pulses of the TAC is proportional to the delay time between the rf trigger pulse and the arrival time of a photon; a pulse-height analysis gives then the time-differential structure of the photon pulses. The result of such an experiment is shown in Fig. 8(b). We observe two maxima of the fluorescence signal per rf period, which reflects the fact that in a two-ion crystal the micromotion of the individual ions is 180° out of phase. Covering one constituent ion of the crystal indeed generates only one maximum per field cycle [see Fig. 8(a)]. The excitation spectrum acts as a transfer function (modulator) for the translation of the velocity modulation into the corresponding variations of fluorescence intensity. For a small velocity modulation amplitude the response in the fluorescence intensity is harmonic. If a linear approximation to the excitation spectrum would be permissible, the fluorescence intensity should be a flat function in Fig. 8(b). The fact that modulations in the fluorescence intensity are clearly present in Fig. 8(b) proves that the amplitude of the micromotion is already so large that the nonlinearities of the excitation spectrum are important. The contact potential, or other asymmetries in the trap field, cause the signals from the individual ions to have different amplitudes. The combined signal is then asymmetric. By applying a compensating

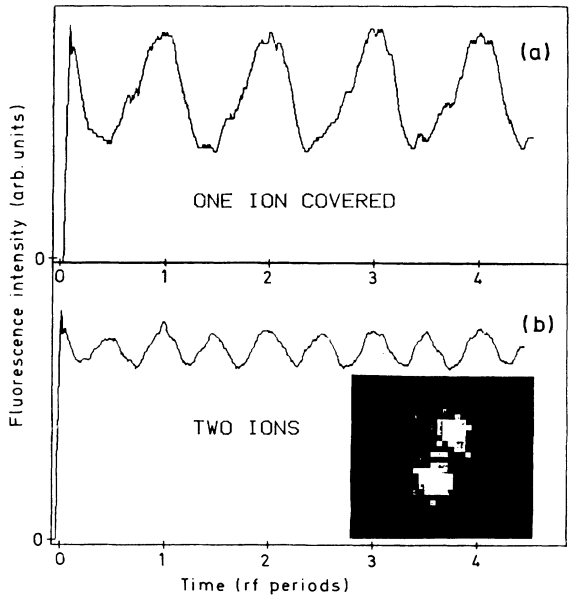

FIG. 8. Time dependence of the fluorescence intensity (in arbitrary units) resulting from the micromotion of the ions in a two-ion crystal close to the center of the trap. The crystal is oriented in the x-y plane (see inset). The laser beam was nearly orthogonal to the crystal axis in the x-y plane. For the upper curve, the signal of one ion was blocked, the lower curve was obtained from the fluorescence light of both ions.

voltage between the caps of the trap, this asymmetry can be equalized. In the measurement shown in Fig. 8(b), a dc voltage of 100 mV was necessary for compensation.

In general, the micromotion corresponds to a frequency modulation of the laser light in the rest frame of the ions. Therefore the excitation spectrum of harmonically moving ions is not just a single Lorentzian, but a sum of saturation broadened Lorentzians, peaked at $\omega=\omega_L\pm n\Omega$ and with a strength proportional to the square of the nth Bessel function:

$$I(\Delta)\sim\sum_{n=-\infty}^{+\infty}\frac{J_n^2(\beta)}{(\Delta+nf)^2+(\Gamma_{\rm sat}/2)^2}\ . \tag{39}$$

In this formula Δ is the laser detuning with respect to the resonance frequency of a single ion at rest, β is the modulation index given by

$$\beta=\frac{\mathbf{k}\cdot\mathbf{v}_0}{\Omega}\ , \tag{40}$$

and $\Gamma_{\rm sat}$ is the power-broadened natural linewidth. The amplitude of the micromotion velocity is denoted by $\mathbf{v}_0$. Figure 9(a) shows the function $I(\Delta)$ in the range $-1<\Delta<1$ GHz. With these parameters, 130 Bessel functions were necessary for convergence, which means that 130 rf sidebands contribute to the final shape of the curve.

Let us now consider a single ion sitting a distance d away from the center of the trap, e.g., an ion in a crystal or a single ion displaced out of the trap's center by an additional dc voltage applied between the end caps of the trap. Such an ion will exhibit strong micromotion, and on time scales larger than one rf period, will lead to the typical double-humped excitation function shown in Fig. 9(a). Suppose that we now choose a laser detuning $\Delta=\Delta_1<0$ left of the first hump of the excitation function, and distort the ions such that on top of the micromotion it exhibits a small-amplitude secular vibration. Due to the Doppler effect this additional velocity component generates a modulation of the detuning in the range $\Delta_1-\delta<\Delta<\Delta_1+\delta$ [width of the hatched area around Δ_1 in Fig. 9(a)] with respect to the rest frame of the ion. Since, to a good approximation, the area under the excitation function in a certain range of detunings Δ is proportional to the number of photons scattered, the area $A_1^{(l)}$, e.g., is proportional to the number of photons scattered while the ion is moving *in* the direction of laser light propagation, and $A_1^{(r)}$ is the number of photons scattered while the ion is moving in the *opposite* direction.

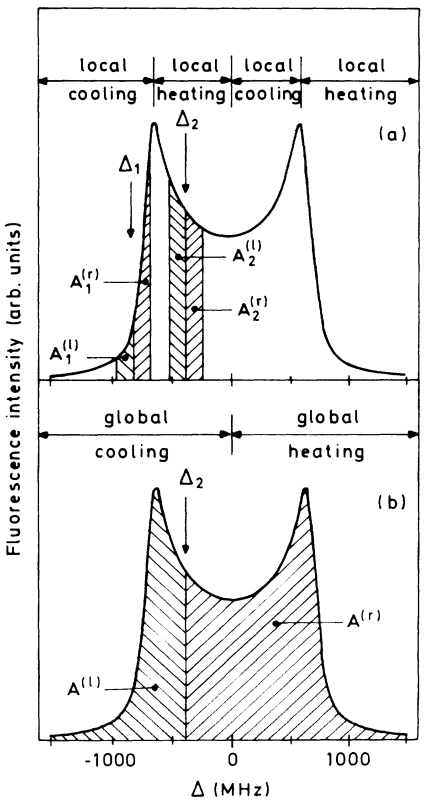

FIG. 9. Synthetic sideband spectrum resulting from the micromotion of an ion displaced from the trap center ($\beta=60$, $f=11.25$ MHz, and $\Gamma_{\rm sat}=150$ MHz). The figure is used for explaining (a) local and (b) global heating and cooling. For details see text.

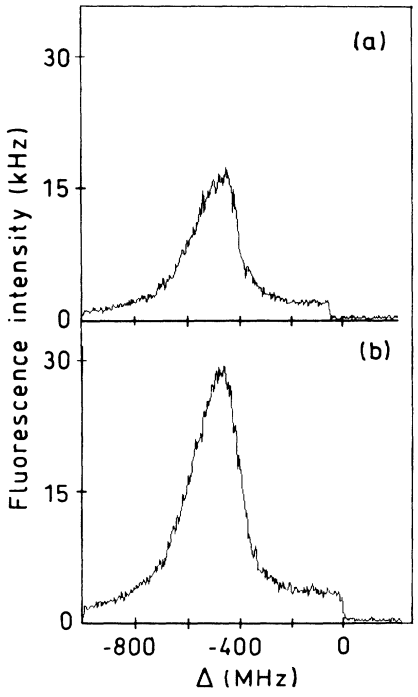

FIG. 10. Experimental sideband spectrum of a single-ion (a) and a two-ion crystal (b). In both cases the ions were displaced 85 μm from the trap center by means of a contact potential. The laser is tuned slowly (5 sec for the total scan) across one ($\Delta<0$) of the two sideband structures. The position of the unshifted resonance frequency is marked by 0. The frequency calibration of the laser light was performed by means of a Doppler-free iodine spectrum before frequency doubling. The parameters are $q=0.044$, $a=0$, and $P=350$ μW. The fluorescence intensity is given in counts per second.

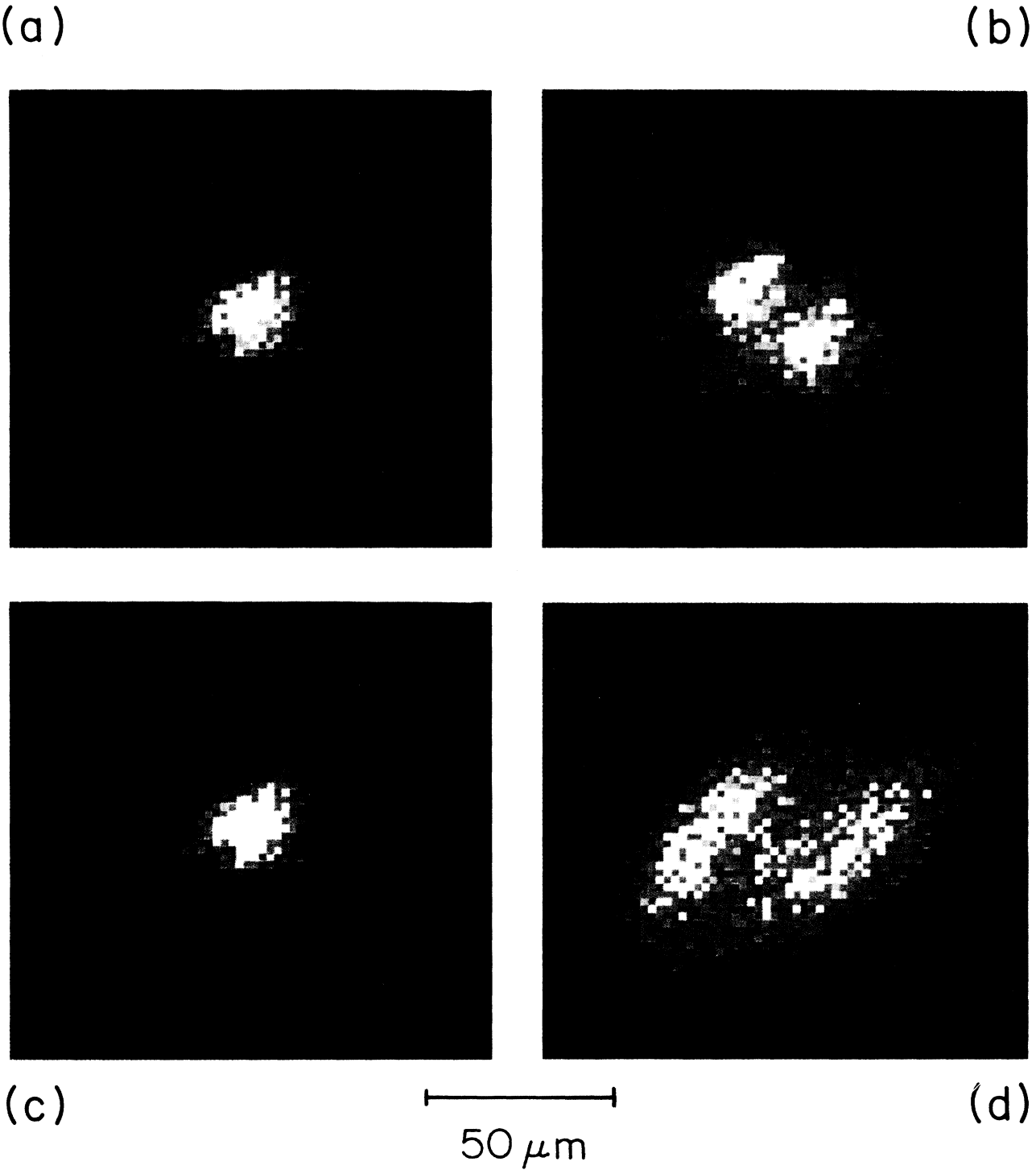

FIG. 11. Secular motion of one and two ions under the influence of local heating and cooling. (a) and (c) show a single ion with the laser tuned to the left (a) and right side (c) of the sideband structure. In the case (c) local heating causes a strong secular motion pointing towards the trap center which is 85 μm away from the equilibrium position. (b) and (d) show the corresponding images for two ions. In this picture, the laser points vertically up→down. The parameters are $q=0.044$, $a=0$, and $P=300$ μW; and (a),(b) $\Delta=-550$ MHz, (c) $\Delta=-300$ MHz, and (d) $\Delta=-330$ MHz. The colors in the plots reflect the intensity of the fluorescence light in percent of maximum fluorescence. Color code: blue, 0–20 %; red, 20–40 %; orange, 40–60 %; yellow, 60–90 %; and white, 90–100 %.

Cooling, therefore, results if $A_1^{(r)} > A_1^{(l)}$, which is fulfilled for $\Delta = \Delta_1$.

In contrast, for $\Delta = \Delta_2$, we have $A_2^{(r)} < A_2^{(l)}$ resulting in a heating of the ion. Naively one could think now that due to this mechanism the ion is finally heated out of the trap. But Fig. 9(b) shows that for very high amplitudes of the motion, i.e., globally, the area $A^{(r)} > A^{(l)}$, resulting in a global cooling of the ion. Apparently we are here in the presence of two counteracting mechanisms which, after some time, will lead to a new equilibrium situation in which the ion is still stored in the trap. The investigation of this new type of ion motion is the subject of the following experiments.[37]

With the help of an additional electric field, a single ion was displaced out of the center of the trap. The radial component of the displacement was $d_x = 60$ μm and $d_y = 60$ μm. The z component was negligible. Here the x and y axes are defined such that the projection of the laser-beam direction on the x-y plane is parallel to the (vertical) y axis and orthogonal to the (horizontal) x axis. The source of the electric field was the contact potential which is always present in our apparatus due to unintentional coating of the ring electrode with the neutral beam of Mg atoms during the loading cycle of the trap. The corresponding fluorescence spectrum of the single ion is shown in Fig. 10(a). At zero detuning, the fluorescence vanishes because the ion is repelled out of the laser focus due to global heating. Detuning the laser to the left of the first hump of the excitation function, we observe the ion in the form of a dot [see Fig. 11(a)]. Detuning the laser to the right of the first hump, the ion heats up and results in the elongated dash shown in Fig. 11(c). The dash represents the new equilibrium situation in which local heating and global cooling balance out. The origin of the elongated appearance of the ion is the secular motion resulting from the local heating. The direction of this secular motion is parallel to the micromotion, i.e., it points to the trap center. Scanning the laser frequency from a large negative detuning toward the atomic resonance frequency, the oscillation amplitude of the ion starts to increase exactly at the top of the first hump where local cooling turns into local heating. Scanning the frequency back again, no hysteresis is observed. With the help of a photon-photon correlation experiment, the nature of this new equilibrium phase can be investigated in more detail and shows clear evidence that the motion of the ion is composed of the micromotion superimposed on the secular motion which was excited by the local heating condition. The results of the correlation experiments are shown in Figs. 12(a) and 12(b). In Fig. 12(a) the laser was tuned to the positive slope of the sideband spectrum [10(a)] and in Fig. 12(b) to the opposite side. In the latter case the secular motion shows up clearly, whereby the time variation is governed essentially by twice the secular frequency of a single ion. The frequency is doubled since the amplitude of the motion causes a Doppler tuning of the laser frequency far beyond the maximum. This result provides further evidence of the existence of global cooling, since otherwise the ion would not stay in the trap.

During the time the ion is oscillating with the secular frequency, the micromotion is changing periodically: It is larger when the ion is further displaced and smaller when the ion is closer to the center. Therefore the sideband spectrum resulting from the micromotion is changing periodically also. An indication of this variation can be seen in Fig. 12(b), since every other maximum of the $G^{(2)}$ signal is larger than the neighboring ones. Figure 12(a) does not show the secular motion, since in this case the laser is tuned to the left side of the sideband maximum where cooling is present. It should be mentioned here that the antibunching[40] cannot be seen in Fig. 12, since the signal recording was started at a time corresponding to 500 times the natural lifetime of the excited state.

The same type of experiment was performed with a crystal consisting of two ions. The crystal was again displaced a distance $d = 85$ μm out of the trap's center and appears as two dots for laser detunings left of the first hump [see Fig. 11(b)]. Tuning the laser to the right of the first hump, the ions perform a synchronized large-amplitude motion which results in the two parallel dashes displayed in Fig. 11(d). A nearly identical excitation function is obtained [see Fig. 10(b)]. Also in the two-ion case a photon-correlation experiment has been performed. The result is shown in Fig. 13. The time scale is different from Fig. 12 so that the micromotion can be seen in addition to the secular motion. It is also obvious

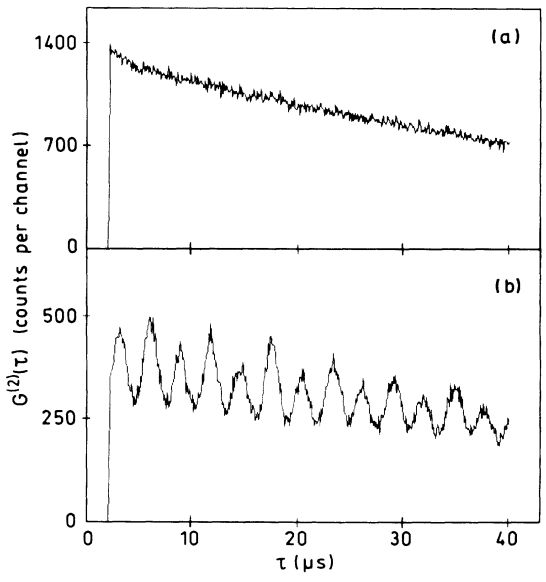

FIG. 12. Photon correlation measurement $[G^{(2)}(\tau)]$ for a single ion displaced 85 μm from the trap center. In (a) the laser was tuned to the left-hand side and in (b) to the right-hand side of the sideband structure. The secular motion of the ion shows up in (b). The frequency displayed is double the frequency of the secular motion for a single ion. In this case the micromotion is not resolved [see Fig. 13(b) for comparison]. More details are given in the text. The slow decrease of $G^{(2)}$ toward larger times is due to the fact that the average counting rate was somewhat too large; this favors a larger signal at shorter times. The parameters are $P = 250$ μW, $q = 0.044$, and $a = 0$; and (a) $\Delta = -600$ MHz and (b) $\Delta = -400$ MHz.

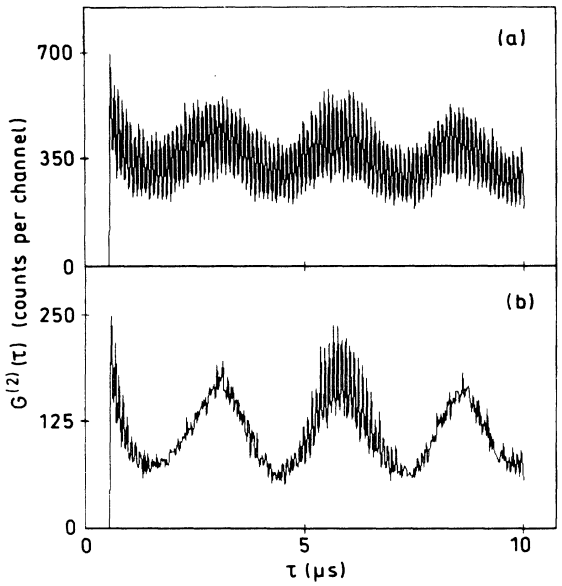

FIG. 13. Photon-correlation measurement $G^{(2)}(\tau)$ for a two-ion crystal (a) and a single ion (b). For this measurement the laser was tuned to the right-hand side of the sideband structure such that local heating is present. The time scale is larger than in Fig. 12, so that the micromotion can be observed. The amplitude of the micromotion is changing periodically with the secular motion depending on the position of the ions in the trap. Except for the detunings, the parameters are as in Fig. 12. (a) $\Delta = -90$ MHz and (b) $\Delta = -120$ MHz.

from the figure that the amplitude of the micromotion changes periodically depending on the position of the two-ion crystal with respect to the trap center. (This effect was mentioned already in connection with the single-ion spectra.) This new type of motion does not represent a melted crystal and so, even in the presence of local sideband heating, two-ion crystals do not melt.

In connection with the heating by the micromotion it is interesting to investigate how much the ion crystals themselves can be affected by this additional heating effect. For this purpose the crystal has to be investigated close to the actual trap center in a situation where no perturbation by a contact potential is present. In order to obtain a controlled displacement, a small voltage is applied between the cap electrodes shifting the ions in the z direction. Measurements with a single ion are shown in Fig. 14(a). The upper curve shows the excitation spectrum when a voltage of 390 mV is applied, leading to a z displacement of 31 μm. The larger micromotion of the displaced ion produces a sideband spectrum with an outer maximum at roughly 200 MHz. A change of the voltage to 625 mV resulting in a displacement of 50 μm shifts the sideband maximum to 600 MHz corresponding to a β of 87. The excitation spectrum of the two-ion crystal (crystal at the trap center) is shown in Fig. 14(b). The spectrum corresponds to the one of a single ion at the trap center, thus demonstrating that the micromotion is negligible in this case. When the light of one of the two ions is blocked, a spectrum is obtained which is up to normalization identical with the two-ion spectrum confirming the negligible influence of the micromotion. It should be mentioned here that the micromotion has also been studied by deVoe, Hoffnagle, and Brewer.[26] In their experiment the ion was displaced in the z direction and a change in the effectiveness of the laser cooling due to the presence of the micromotion was observed by measuring the amplitude of secular oscillations which were excited by an additional ac voltage applied to the trap electrodes.

In summary we can say that although a proper order→chaos transition might be encountered for $q_c > q_{MI}$, this transition cannot be observed since the motion in the trap becomes globally unstable at $q = q_{MI}$, where the ions fall out of the trap. For an order→chaos transition to occur, the system has to be kicked by an external perturbation from the nonheating, quasiperiodic region of phase space into the chaotic, heating region. The location of the order→chaos transition points are therefore of no physical relevance, since they merely

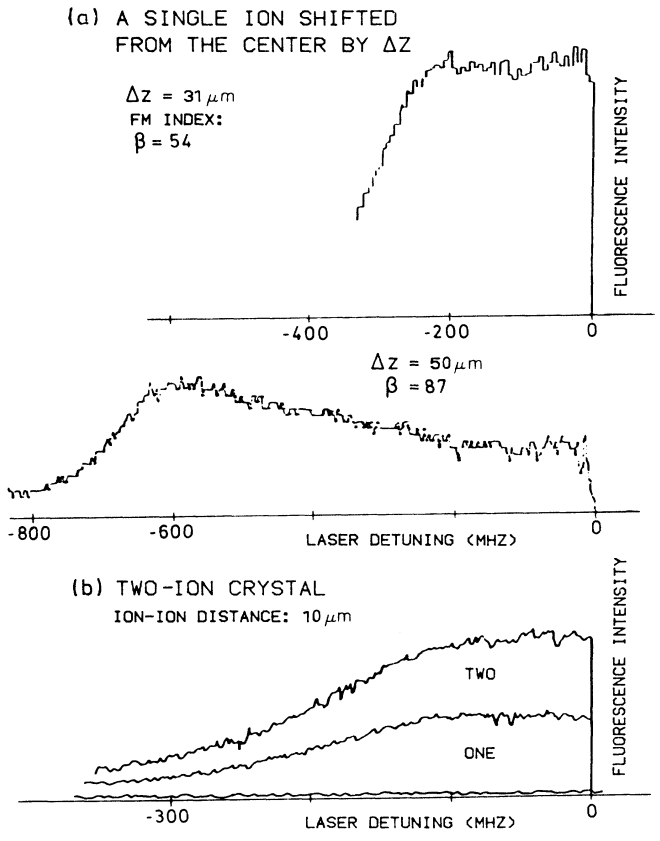

FIG. 14. (a) Sideband spectrum of a single ion shifted in the z direction by applying a dc voltage between the cap electrodes. The displacement of the ion is $\Delta z = 31$ μm and $\Delta z = 50$ μm, respectively. In this case, the influence of the contact potential was negligible since the trap potential was much steeper than in the case of Fig. 10. (b) Spectrum of a two-ion crystal in the center of the trap (negligible contact potential and no additional voltage applied). The lower curve was obtained when the fluorescence light of one of the ions was blocked. The spectrum shows negligible influence of the micromotion.

reflect the strength of the uncontrolled external perturbation which provides the energy to bridge the gap between heating and nonheating phase-space domains.

Crystal melting might be assisted by local laser heating and since the heating effect depends on the amplitude of the micromotion, a proper chaos transition in the presence of the laser light might be encountered for very large crystals. For small crystals we did not observe such a transition, but saw clear evidence for the presence of local laser heating which reflects itself in the large amplitude vibrations of a single-ion and a two-ion crystal in Figs. 11(c) and 11(d), respectively. While in this section we concentrated mainly on the regular phase-space domains and the order→chaos transition, Sec. VI will focus mainly on the chaotic phase-space domains and the chaos→order transition.

VI. THE rf HEATING MECHANISM

The rf heating mechanism is concealed in the properties of the equations of motion (21), and major results concerning this mechanism have already been presented in Refs. 15–17. Here we attempt a more detailed and a more quantitative treatment and show new results, which support the general ideas outlined in Ref. 15. In order to unravel the origin of rf heating, one might think of investigating simpler versions of (21), e.g., a one-dimensional string of ions subjected to nothing but the rf trap force and the mutual Coulomb repulsion. Whether the simplified one-dimensional model of the ion trap reveals the origin of the rf heating mechanism is answered by the following numerical experiment: We integrated the x component of (21) and monitored the average kinetic energy of two to five ions as a function of time. For less than five ions we could not observe any gain in energy over several tens of milliseconds. For five ions a slow increase in energy was recorded, unfortunately too small to account for the stability of ion clouds in the presence of laser cooling. A fast-Fourier transform of the positions $x_n(j)$ of the nth member of the one-dimensional ion chain taken at discrete times $t_j = jT$

$$P_k^{(n)} = \frac{1}{\sqrt{N}} \sum_{j=0}^{N-1} x_n(j) \exp\left[-i \frac{2\pi}{N} jk \right], \quad k = 0, 1, \ldots, N-1 \tag{41}$$

($N = 2048$ in the present case) shows a small number of discrete frequencies dominating the spectrum, thus qualifying this model as being close to integrable and lacking a heating mechanism. Although the one-dimensional chain of particles cannot be used to explain the heating mechanism in a Paul trap, it is interesting in its own right and closely related to the integrable chain of particles interacting by two-body harmonic and $1/x^2$ potentials (Calogero-Moser system[41,42]).

Two-dimensional ion traps behave essentially like one-dimensional traps if the motion is restricted to the x-y plane. In the x-z (y-z) plane, however, strong heating occurs. In order to study this observation in more detail, we have calculated the power spectrum $|P_k|^2$ of the positions of two ions. As already shown in Sec. IV there is always a small phase-space region around the crystalline solution in which no heating occurs (compare Fig. 5). The power spectrum is discrete in this case, typical for quasiperiodic motion. In the quasiperiodic phase, the ions are unable to extract energy from the rf field and if a cooling laser is present, they eventually end up in the crystalline state. Such a power spectrum characterizes phase-space domains which act as basins of attraction for the crystal (see white regions in Fig. 5). However, when we choose initial conditions, which correspond to typical separations in a cloud state [dotted regions in Fig. 5(a)], the spectral power of any one of the two ions shows continuous bands in frequency. This provides evidence for the occurrence of deterministic chaos[43] in the cloud phase.

For a quantitative investigation of chaotic rf heating, we calculated the work done by the rf field per unit time (angular brackets denoting ensemble averages)

$$\kappa = f\left\langle \sum_{i=1}^{n} \int_{1\,\text{cycle}} \mathbf{F}_i^{(\text{trap})} \cdot d\mathbf{s}_i^{(\text{ion})} \right\rangle = f\left\langle \sum_{i=1}^{n} \int_0^T \mathbf{F}_i^{(\text{trap})} \cdot \mathbf{v}_i^{(\text{ion})} dt \right\rangle \tag{42}$$

for the case $n = 5$ ions, $V_0 = 780$ V, $U_0 = 0$, $f = 11.25$ MHz, and $\Delta = -300$ MHz as a function of the rms radius $r = (\overline{r^2})^{1/2} = \langle (\sum_{i=1}^{n} \mathbf{r}_i^2)^{1/2} \rangle$ of the five ions. The rms radius was controlled indirectly by the laser power P which we varied from 10 to 150 μW to obtain the heating curve[17] displayed in Fig. 15. For zero laser power and large r, we did not observe any net heating of the ions. This is confirmed by our experiments, in which, even in the absence of a cooling laser, large clouds of ions can be stored in a Paul trap over several hours without being heated out of the trap. The ions are far apart from each other, the Coulomb force is small, and on short time scales the ions behave essentially like independent single stored ions. For this reason, we called this part of the heating diagram the "Mathieu regime." Turning on a small laser power, the rms radius r reduces drastically, but comes to a halt at about 14 μm where chaotic rf heating sets in and balances the cooling power of the laser. Increasing the laser power results in an even smaller cloud. The smaller cloud produces more chaotic rf heating, as seen clearly by the negative slope of the heating curve (Fig. 15) in the range $8 < r < 14$ μm.

In the range $4 < r < 8$ μm there is still chaotic heating but the slope of the heating curve is positive. As a consequence of the resulting triangular shape of the heating curve at about $P = 150$ μW, corresponding to $r \approx 8$ μm, the chaotic heating power can no longer balance the cooling power of the laser and the cloud collapses into the crystalline state located at $r \approx 3.8$ μm. A phase transition has occurred. Since the rf heating power depends on a and q and the laser cooling power on P and Δ, the occurrence of the cloud→crystal transition is a rather complicated function of a, q, P, and Δ. Due to this collapse of the cloud state, the behavior of the heating rate in the range $3.8 < r < 8$ μm cannot be studied by equilibrating laser cooling and rf heating. In this case we start out

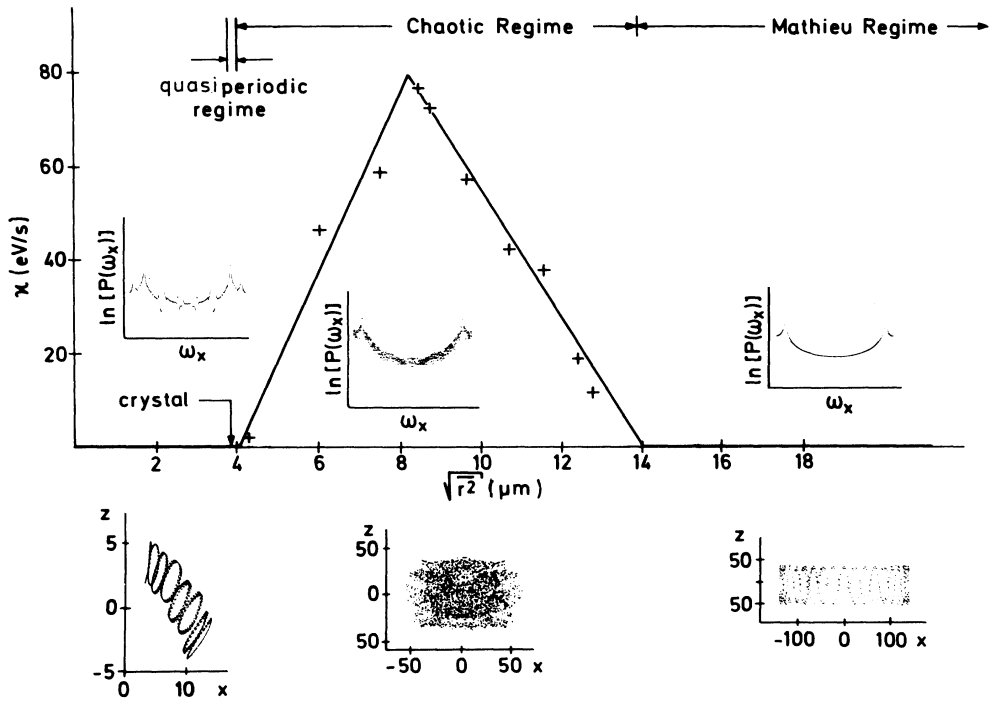

FIG. 15. Average heating rate κ of five ions in a Paul trap vs the rms radius of the ion configuration. The insets show the power spectrum and the corresponding stroboscopic Poincaré sections in the x-z plane of relative separation for two ions in three characteristic domains: the quasiperiodic regime, the chaotic regime, and the Mathieu regime. All length scales are in units of micrometers.

from the crystal state and slightly displace the ions to explore the vicinity of the crystal. We observe no heating for $3.8 < r < 4$ μm, but quasiperiodic motion, and thus dubbed this regime the "quasiperiodic" regime. We call the upper edge of the quasiperiodic regime ($r \approx 4$ μm) the "chaos threshold." An initial condition beyond the chaos threshold, i.e., satisfying $r > 4$ μm, leads to heating, and expansion of the ion configuration and numerical data relevant for the shape of the heating curve can be taken during this explosion phase. The laser power P is set to zero for this type of experiment. We conjecture that, apart from the trivial case of a single stored ion, the heating curve is universal, i.e., its qualitative shape, including the existence of the chaotic regime, does not depend on the number of simultaneously trapped ions, and, as already mentioned in the Introduction, even applies to systems as remotely connected as, e.g., Rydberg atoms in strong electromagnetic fields.

For the quasiperiodic, the chaotic, and the Mathieu regimes, respectively, we display the corresponding type of power spectrum as the insets above the abscissa of Fig. 15. The data were actually taken for the case of two ions, but would not look much different in the five-ion case. We obtain a discrete spectrum in the quasiperiodic regime and a complicated noisy spectrum in the chaotic regime. The spectrum in the Mathieu regime is again quite simple and dominated by the secular motion frequency. We also show stroboscopic pictures of the locations of the ions in the x-y plane of the trap characterizing the three regions (insets below the abscissa of Fig. 15).

As a function of increasing rf voltage, the chaos threshold moves towards the radius of the crystalline configuration. However, before the chaos threshold reaches the crystal radius, the equations of motion (21) become unstable in z direction, indicating that in this particular situation the particles would fall out of the trap. In order to achieve proper melting without losing particles, the crystal radius has to be enlarged artificially by noise so that the size of the distorted crystal overlaps with the region of chaotic heating. Proper melting without the assistance of noise should be possible if we start in a quasiperiodic state typified in the bottom left inset of Fig. 15. Such configurations have a larger radius to begin with, and the chaos threshold could be reached before the single-particle Mathieu instability sets in.

An interesting numerical experiment concerned replacing the $1/r$ Coulomb repulsion between ions by a screened Coulomb (Yukawa) potential $e^{-r/\alpha}/r$, where α was set to 2 μm. This replacement did not change the cloud$\rightarrow$crystal transition points, and we conclude that the heating properties of an ion cloud do not depend sensitively on the long-range properties of the ion-ion potential. Heating, i.e., energy gain, seems to originate from very close ion-ion collisions. This observation offers another possibility for future research: the investigation of the heating properties of a hard-sphere gas and its comparison to the heating properties of the more conventional Coulomb gas confined in a trap.

We conclude this section by briefly comparing the rf heating mechanism in a Paul trap with the ionization

mechanism of Rydberg atoms in strong microwave fields (compare also ref. 15). In both cases, heating, i.e., absorption of energy from the driving field, heavily relies on the occurrence of chaotic motion. But in contrast to the situation in ion traps, a proper order→chaos transition marks the onset of strong ionization in the case of Rydberg atoms. Diffusing models similar to the ones developed for Rydberg atoms[9] should be designed in order to obtain the energy diffusion coefficient, which allows for an analytical calculation of the steady-state size of ion clouds and the exact location of the cloud→crystal (chaos→order) phase-transition points.

VII. CONCLUSION

In this paper we present a detailed theoretical and experimental study of the transition of few ion crystals into clouds. It could be shown that this transition cannot be described as an order→chaos transition occurring at a critical value of a control parameter. The crystalline phase can exist until the Mathieu instability limit is reached. When this limit is approached, the system becomes very sensitive to perturbations, so that the melting of the crystal can be observed well before the instability limit.

In addition, we discussed the influence of the micromotion on the stability of the crystals. Additional heating and cooling by the micromotion could be demonstrated. The effects are, however, only relevant if the ions are strongly displaced from the trap center. Crystals with a small number of ions are not affected by the micromotion so that these effects are only of minor importance for the transitions between the crystalline and cloud phases.

In detailed studies of one-, two-, and three-dimensional simulations of ions in a Paul trap, we have shown that depending on the radius of the ion arrangement, the dynamics of ions in a Paul trap can be classified into four dynamical regimes: (i) the crystal, (ii) the quasiperiodic regime, (iii) the chaotic regime, and (iv) the Mathieu regime. The crystal, the quasiperiodic regime, and the Mathieu regime are the nonheating regimes. Strong heating occurs only in regime (iii) by a diffusive gain of energy due to the occurrence of deterministic chaos.

[1]M. J. Feigenbaum, Phys. Lett. **74A**, 375 (1978); J. Stat. Phys. **19**, 25 (1978); **21**, 669 (1979).

[2]G. Casati, B. V. Chirikov, F. M. Izrailev, and J. Ford, in *Stochastic Behavior of Classical and Quantum Hamiltonian Systems*, Vol. 93 of *Lecture Notes in Physics*, edited by G. Casati and J. Ford (Springer, Berlin, 1979), p. 334.

[3]S. Fishman, D. R. Grempel, and R. E. Prange, Phys. Rev. Lett. **49**, 509 (1982); D. R. Grempel, R. E. Prange, and S. Fishman, Phys. Rev. A **29**, 1639 (1984).

[4]R. Blümel, S. Fishman, and U. Smilansky, J. Chem. Phys. **84**, 2604 (1986).

[5]H. Frahm and H. J. Mikeska, Z. Phys. B **65**, 249 (1986).

[6]R. Scharf, B. Dietz, M. Kuś, F. Haake, and M. V. Berry, Europhys. Lett. **5**, 383 (1988).

[7]R. Blümel and U. Smilansky, Phys. Rev. Lett. **52**, 137 (1984).

[8]T. Dittrich and R. Graham, Z. Phys. B **62**, 515 (1986).

[9]N. B. Delone, B. P. Krainov, and D. L. Shepelyansky, Usp. Fiz. Nauk. **140**, 355 (1983) [Sov. Phys.—Usp. **26**, 551 (1983)].

[10]G. Casati, B. V. Chirikov, D. L. Shepelyansky, and I. Guarneri, Phys. Rep. **154**, 77 (1987).

[11]R. Blümel and U. Smilansky, Z. Phys. D **6**, 83 (1987).

[12]J. E. Bayfield and D. W. Sokol, Phys. Rev. Lett. **61**, 2007 (1988).

[13]E. J. Galvez, B. E. Sauer, L. Mooreman, P. M. Koch, and D. Richards, Phys. Rev. Lett. **61**, 2011 (1988).

[14]J. Hoffnagle, R. G. DeVoe, L. Reyna, and R. G. Brewer, Phys. Rev. Lett. **61**, 255 (1988).

[15]R. Blümel, J. M. Chen, E. Peik, W. Quint, W. Schleich, Y. R. Shen, and H. Walther, Nature **334**, 309 (1988).

[16]R. Blümel, J. M. Chen, F. Diedrich, E. Peik, W. Quint, W. Schleich, Y. R. Shen, and H. Walther, in *Proceedings of the Eleventh International Conference on Atomic Physics (ELICAP), Paris, 1988*, edited by J. C. Gay (World Scientific, Singapore, 1989).

[17]R, Blümel, J. M. Chen, F. Diedrich, E. Peik, W. Quint, and H. Walther, *Quantum Optics V*, Vol. 41 of *Springer Proceedings*, edited by D. F. Walls and J. D. Harvey (Springer, Berlin, 1989).

[18]F. Diedrich, J. C. Bergquist, W. M. Itano, and D. J. Wineland, Phys. Rev. Lett. **62**, 403 (1989).

[19]A. Holle, J. Main, G. Wiebusch, H. Rottke, and K. H. Welge, Phys. Rev. Lett. **61**, 161 (1988).

[20]R. Blümel, R. Graham, L. Sirko, U. Smilansky, H. Walther, and K. Yamada, Phys. Rev. Lett. **62**, 341 (1989).

[21]D. Habs, in *Frontiers of Particle Beams*, edited by M. Month and S. Turner (Springer, Berlin, 1988).

[22]J. P. Schiffer and P. Kienle, Z. Phys. A **321**, 181 (1985).

[23]A. Rahman and J. P. Schiffer, Phys. Rev. Lett. **57**, 1133 (1986).

[24]J. P. Schiffer and O. Poulsen, Europhys. Lett. **1**, 55 (1986).

[25]M. Hénon and C. Heiles, Astron. J. **69**, 73 (1964).

[26]R. G. DeVoe, J. A. Hoffnagle, and R. G. Brewer, Opt. News **14**, 218 (1988); R. G. DeVoe (private communication).

[27]F. Diedrich, E. Peik, J. M. Chen, W. Quint, and H. Walther, Phys. Rev. Lett. **59**, 2931 (1987).

[28]D. Wintgen and H. Friedrich, Phys. Rev. Lett. **57**, 571 (1986).

[29]R. Blümel and U. Smilansky, Phys. Rev. Lett. **58**, 2531 (1987).

[30]W. Paul, O. Osberghaus, E. Fischer, Forschungsber. Wirtsch. Verkehrsminist. Nordrhein Westfalen **415**, 1 (1958).

[31]E. Fischer, Z. Phys. **156**, 1 (1959).

[32]R. F. Wuerker, H. Shelton, and R. V. Langmuir, J. Appl. Phys. **30**, 342 (1959).

[33]H. G. Dehmelt, Adv. Atom. Mol. Phys. **3**, 53 (1967); **5**, 109 (1969).

[34]D. J. Wineland, J. C. Bergquist, W. M. Itano, J. J. Bollinger, and C. H. Manney, Phys. Rev. Lett. **59**, 2935 (1987).

[35]W. T. Reid, *Ordinary Differential Equations*, (Wiley, New York, 1971), pp. 440–445, P. M. Morse and H. Feshbach, *Methods of Theoretical Physics* (McGraw-Hill, New York, 1953), Pt. I, p. 557.

[36]A. J. Lichtenberg and M. A. Lieberman, *Regular and Stochastic Motion*, Vol. 38 of *Applied Mathematical Sciences* (Springer, New York, 1983).

[37]W. Quint, Ph. D. thesis, Ludwig-Maximilians Universität,

München, 1989.
[38]B. B. Mandelbrot, Physica D **7**, 224 (1983).
[39]H. O. Peitgen and P. H. Richter, *The Beauty of Fractals* (Springer, Berlin, 1986).
[40]F. Diedrich and H. Walther, Phys. Rev. Lett. **58**, 203 (1987).
[41]F. J. Calogero, Math. Phys. **12**, 419 (1971).
[42]J. Moser, Adv. Math. **16**, 1 (1975).
[43]H. G. Schuster, *Deterministic Chaos* (Physik-Verlag, Weinheim, 1984).

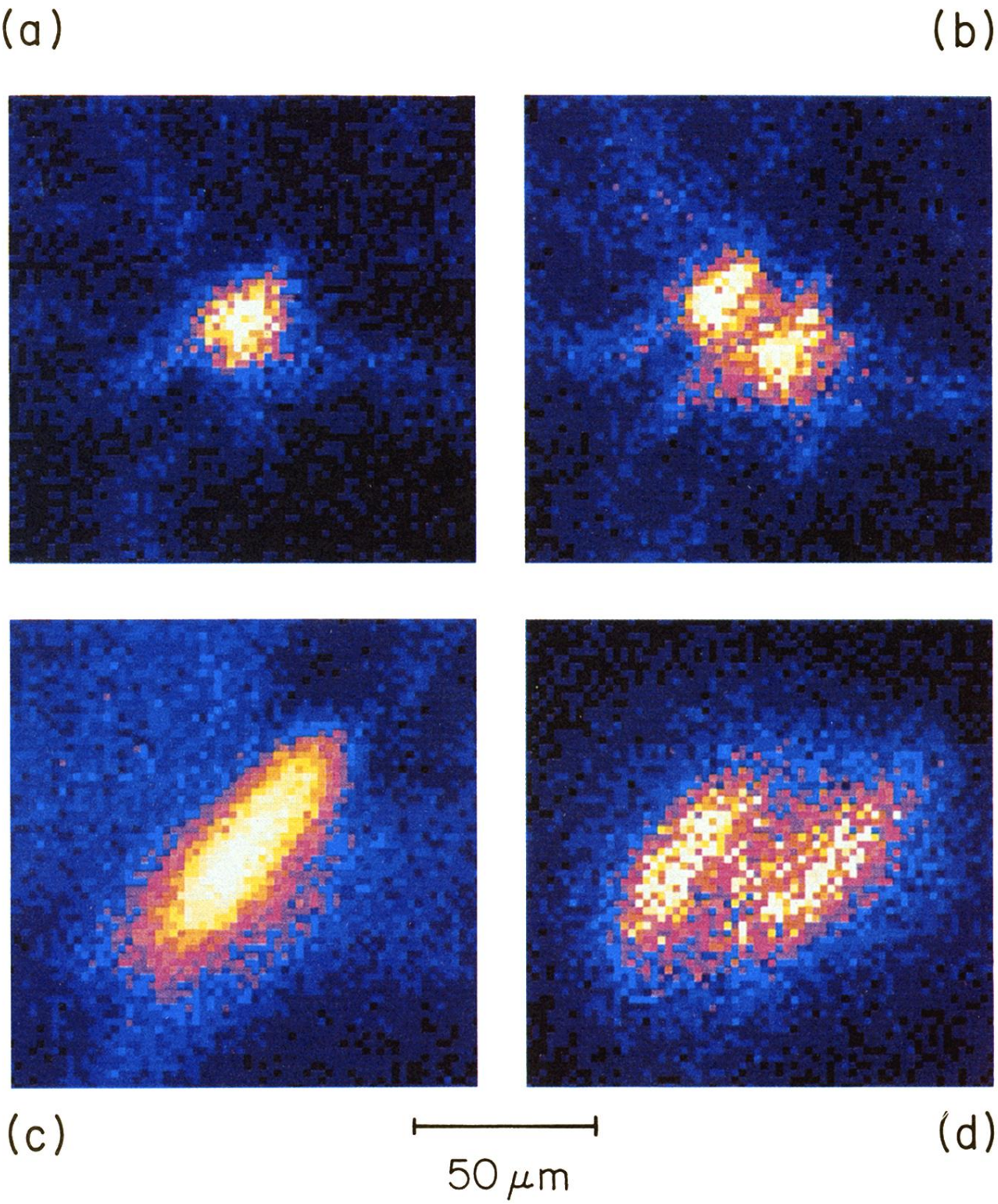

FIG. 11. Secular motion of one and two ions under the influence of local heating and cooling. (a) and (c) show a single ion with the laser tuned to the left (a) and right side (c) of the sideband structure. In the case (c) local heating causes a strong secular motion pointing towards the trap center which is 85 μm away from the equilibrium position. (b) and (d) show the corresponding images for two ions. In this picture, the laser points vertically up→down. The parameters are $q=0.044$, $a=0$, and $P=300$ μW; and (a),(b) $\Delta=-550$ MHz, (c) $\Delta=-300$ MHz, and (d) $\Delta=-330$ MHz. The colors in the plots reflect the intensity of the fluorescence light in percent of maximum fluorescence. Color code: blue, 0–20 %; red, 20–40 %; orange, 40–60 %; yellow, 60–90 %; and white, 90–100 %.